Fate of Springtime Atmospheric Reactive Mercury: Concentrations and Deposition at Zeppelin, Svalbard

Stefan Osterwalder, Sarrah Dunham-Cheatham, Beatriz Ferreira Araujo, Olivier Magand, Jennie Thomas, Foteini Baladima, Katrine Aspmo Pfaffhuber, Torunn Berg, Lei Zhang, Jiaoyan Huang, et al.

Fate of Springtime Atmospheric Reactive Mercury: Concentrations and Deposition at Zeppelin, Svalbard

Author(s):
Osterwalder, Stefan; Dunham-Cheatham, Sarrah M.; Ferreira Araujo, Beatriz; Magand, Olivier; Thomas, Jennie L.; Baladima, Foteini; Pfaffhuber, Katrine Aspmo; Berg, Torunn; Zhang, Lei; Huang, Jiaoyan; Dommergue, Aurélien; Sonke, Jeroen E.; Sexauer Gustin, Mae

Publication date:
2021-11-18

Permanent link:
https://doi.org/10.3929/ethz-b-000512564

Originally published in:
ACS Earth and Space Chemistry 5(11), https://doi.org/10.1021/acsearthspacechem.1c00299

Fate of springtime atmospheric reactive mercury: Concentrations and deposition at Zeppelin, Svalbard

Stefan Osterwalder[1,2*], Sarrah M. Dunham-Cheatham[3], Beatriz Ferreira Araujo[4], Olivier Magand[1], Jennie L. Thomas[1], Foteini Baladima[1], Katrine Aspmo Pfaffhuber[5], Torunn Berg[6], Lei Zhang[7], Jiaoyan Huang[8], Aurélien Dommergue[1], Jeroen E. Sonke[4], Mae Sexauer Gustin[3]

[1] Institut des Géosciences de l'Environnement, Université Grenoble Alpes, CNRS, IRD, Grenoble INP, 460 Rue de la piscine, 38400 Saint-Martin-d'Hères, France
[2] Institute of Agricultural Sciences, ETH Zurich, Universitätstrasse 2, 8092 Zurich, Switzerland
[3] Department of Natural Resources and Environmental Sciences, University of Nevada, 1664 N. Virginia Street Reno, NV 89557, USA
[4] CNRS, IRD, CET, Université Paul Sabatier–Toulouse III, Observatoire Midi-Pyrénées 14, avenue Édouard Belin 31400 Toulouse, France
[5] Norwegian Institute for Air Research, Instituttveien 18, 2007 Kjeller, Norway.
[6] Department of Chemistry, Norwegian University of Science and Technology, Gløshaugen, 7491 Trondheim, Norway
[7] School of the Environment, Nanjing University, 163 Xianlin Avenue, Nanjing, Jiangsu 210023, China
[8] Sonoma Technology, 1450 N. McDowell Blvd., Suite 200, Petaluma, California 94954, USA

*corresponding author: stefan.osterwalder@usys.ethz.ch

KEYWORDS:

Aerohead, Arctic, Pollution, RMAS, Speciation, Thermal desorption

Abstract

Mid-latitude atmospheric elemental mercury (Hg) emissions undergo extensive oxidation to reactive Hg (RM) compounds during Arctic polar sunrise, resulting in enhanced atmospheric deposition that impacts Arctic marine wildlife and humans. It has been difficult to estimate RM dry deposition, because RM concentrations, compounds, and their deposition velocities are ill-defined. Here we investigate RM concentrations sampled with membrane-based methods, and find these to exceed denuder-based RM detection by 5 times at the Zeppelin Observatory on Svalbard (March 26 – July 24, 2019). Measured dry deposition of GOM was about half of modeled RM deposition demonstrating that particulate-bound Hg was an important component of dry deposition. Using thermal membrane desorption RM chemistry was found to be dominated by Hg–Cl/Br (51%) and Hg–N (45%) compounds. Back trajectory analysis indicated that Hg–Br/Cl compounds were predominantly advected from within the marine boundary layer (sea ice exposure), while Hg–N originated from the free troposphere. Weekly average RM compound-specific dry deposition velocities ranged from 0.12 to 0.49 cm s^{-1}, with a net RM dry deposition of 1.9 µg m^{-2} (1.5 – 2.5 µg m^{-2}; 95% confidence interval), that exceeds the mean annual Hg wet deposition flux in Svalbard. Overall, we find that springtime atmospheric RM deposition has been underestimated in the Arctic marine environment.

SYNOPSIS:

Atmospheric reactive mercury measurements at Svalbard demonstrate elevated deposition to Arctic ecosystems (5.6-times), and input of Hg-N and halogenated compounds.

1. Introduction

Mercury (Hg) pollution in the Arctic is of concern, because indigenous people rely heavily on marine-based diets that expose them to neurotoxic methylmercury[1,2]. Globally, the toxic burden of anthropogenic Hg pollution for human and ecosystem health is accepted by policy makers, and has resulted in the UNEP Minamata Convention that aims to reduce human and ecosystem exposure to Hg[3]. However, to evaluate the effectiveness of the Convention we must improve our understanding on how Hg cycles between air, land, water, ice, and snow, especially in vulnerable ecosystems, such as the Arctic[4]. The uncertainty in estimates of atmospheric Hg deposition as gaseous elemental Hg (GEM), gaseous oxidized Hg (GOM), or as particulate-bound Hg (PBM) to the Arctic Ocean is illustrated by a comparison of two global numerical Hg models. The GEOS-Chem model[4] suggested an atmospheric Hg input to the Arctic Ocean of 76 Mg yr^{-1}, while the GRAHM model estimated 108 Mg yr^{-1} [5].

The discovery of coastal springtime atmospheric Hg depletion events (AMDEs) in 1995 indicated that reactive Hg (RM = GOM + PBM) dry deposition was an important pathway for atmospheric Hg inputs to Arctic marine ecosystems[6]. Subsequent studies suggested that during AMDEs about 100 Mg RM yr^{-1} was deposited to Arctic snow and ice[7,8]. Oxidation of GEM to GOM during AMDEs is primarily induced by photochemical activation of sea ice-derived halogen compounds[8,9]. In particular, bromine oxide and atomic bromine radicals (BrOx, BrO, Br•) lead to the destruction of ozone (O_3) and oxidation of GEM, with subsequent depletion of both GEM and O_3 in the Arctic atmosphere during polar sunrise[10,11]. Most recently, Obrist et al.[12] found that RM dry deposition to coastal Arctic tundra was substantial during springtime AMDEs, depositing 0.8 – 2.8 μg m^{-2} yr^{-1}. Dry deposition of RM during AMDEs results in higher total Hg concentrations in snow[13,14] that can be followed by re-emission of Hg^0 after photo-reduction[2,15,16]. Approximately 90% of the total Hg in snow can be re-emitted back to the atmosphere after AMDEs[1].

To assess the total input of Hg to Arctic ecosystems during AMDEs, it is crucial to improve RM dry deposition estimates. This could be done by measuring ambient RM concentrations and applying the values in dry deposition models or identifying RM compounds in ambient air and applying compound-specific deposition velocity calculations based on local meteorological data. The spatial resolution of Arctic RM measurements is limited, and the widely used measurement technique to quantify atmospheric Hg (Tekran® speciation system [Tekran® 2537/1130/1135]; Tekran® Instrument Corp., Ontario, Canada) has been demonstrated to underestimate RM by a factor of 2 to 13 in the planetary boundary layer[17-24], and by a factor of 1.6 in the free troposphere[25]. Other studies suggest measurement artefacts for PBM are generated by temperature and collection time[26-28]. Selective collection and analysis of particles smaller than 2.5 μm diameter with the Tekran® also raises the question of the possible underestimation of PBM concentrations[29] particularly in oceanic environments where the RM compounds are dominantly associated with larger (2 – 10 μm) marine aerosols[30,31].

The University of Nevada, Reno – Reactive Mercury Active System 2.0 (RMAS), with cation exchange membranes (CEM) and nylon membranes[32], in combination with a down-facing aerodynamic sampler housing that also uses CEMs (Aerohead sampler)[33,34], have been shown to improve RM concentration measurements, and GOM and RM dry deposition estimates, respectively, relative to the Tekran® 2537/1130/1135 system [35]. These measurement methods have never been applied in the Arctic, though they are necessary since a low bias in RM deposition would lead to underestimation of Hg transfer from the atmosphere to marine and terrestrial ecosystems during AMDEs. Using the RMAS, the chemistry of RM compounds can be suggested using thermal desorption of nylon membranes and subsequent peak deconvolution[20,21,32,36]. This methodology allows for understanding if specific compounds namely HgO, Hg-Br/Cl (e.g. $HgBr_2$, $HgCl_2$), Hg-nitrogen (e.g., $Hg(NO_3)_2$), and Hg-sulfur (e.g., $HgSO_4$), as well as some organic-bound compounds (e.g., MeHg)[24] are present. Knowledge about the chemistry of RM improved local estimates of RM deposition at a coastal research site in Florida, USA[36]. Estimates of dry deposition were based on compound-specific deposition velocity calculations using a multiple resistance model that was developed by Zhang et al.[37] and modified by Lyman et al.[33].

Explaining the bias in atmospheric RM concentration among different measurement methods, in combination with better identification of chemical compounds of RM, has been identified as a top priority task to improve the determination of RM dry deposition from local to global scales[18]. Here we present a procedure to determine RM compound-specific dry deposition velocities in order to calculate springtime RM dry deposition in the Ny-Ålesund area on Svalbard. The goals of the study were to: 1) intercompare RM concentrations using automated (Tekran®) and manual methods (RMAS); 2) identify RM compounds by thermal desorption procedures; 3) investigate the source of RM compounds using back-trajectory analysis; and 4) calculate RM compound-specific dry deposition velocities and compare them with dry deposition measurements made by the Aerohead sampler. The incorporation of new observations of RM concentration, chemistry and compound-specific dry deposition velocities is a necessary intermediate step toward substantially improving numerical models of Hg cycling in the Arctic.

2. Material and Methods

2.1 Location and sampling

Air measurements were carried out from March 26 (11:00) to July 24 (08:00), 2019 at the Zeppelin Observatory (Zeppelin), located on Svalbard in the Norwegian Arctic. The atmospheric research and monitoring station was located on Zeppelin Mountain at 474 m a.s.l. (78.90°N, 11.88°E). The observatory was situated far from major air pollution sources, and thus, was within an undisturbed Arctic environment. A steep downhill slope faced north towards the research village of Ny-Ålesund, a small settlement with 35 to 185 inhabitants at 2 km from the sampling site. The station was operated by the Norwegian Institute for Air Research (NILU) in close collaboration with the Norwegian Polar Institute (NPI). Air inlets for all air Hg measurements were installed 3 m above ground in close proximity to one another, facing downward and toward the predominant wind direction (ESE). Automated atmospheric Hg measurements were carried out by Norwegian University of Science and Technology (NTNU) in collaboration with NILU; manual sampling for RM analyzes was performed by NPI staff. Previous analysis of automated atmospheric Hg and snow Hg measurements at Zeppelin were reported by Dommergue et al.[13], Berg et al.[38-40], Aspmo et al.[41], Gauchard et al.[42], Sprovieri et al.[43,44], Sommar et al.[45], Ferrari et al.[46], Steen et al.[47], and Angot et al.[48].

2.2 Automated GEM and RM measurements

During the campaign, a Tekran® measured GEM, GOM, and PBM continuously following methods briefly described in section S1 and detailed in Landis et al.[49]. The only deviation from the standard operation procedures[50,51] was calculating GOM with the flush blank concentrations added to the GOM measurement; this was done because adding the Tekran® flush blank to RM (GOM + PBM) measurements resulted in a good agreement with manual RM measurements using polyethersulfone membranes at the high altitude Pic du Midi Observatory[25].

2.3 Manual RM measurements

Three different sorption surface materials were used to sample RM. Polyethersulfone membrane (PES, 47 mm diameter, 0.45 μm pore size; Millipore) were previously applied[25,52] and showed a similar sorption capacity and background Hg contents to CEM[53]. The PES and CEM (PES backbone that has been proprietarily treated, 47 mm diameter, 0.8 μm pore size; Mustang-S, Pall Corporation) were applied extensively in recent studies (e.g., Gustin et al.[19]; Marusczak et al.[25]; Luippold et al.[32], Miller et al.[54]) and were deemed the preferable material for quantitative RM measurements due to the high RM sorption efficiency[53]. Nylon membranes (47 mm diameter, 0.2 μm pore size; Sartorius Stedium) were used to determine the chemistry of RM using thermal desorption procedures[19,24]. The chemistry of the RM compounds captured on the nylon membranes was determined by comparing membrane Hg desorption profiles from Svalbard with those developed for standard Hg compounds (see section 2.4 also).

2.3.1 PES measurements

The PES sampling configuration captured RM in ambient air by pumping at 1 L min^{-1} (Membrane vacuum pump, KNF) through a one-stage outdoor filter pack protected from snow fall. The airflow was regulated by a ball flow meter (Fisher Scientific) and quantified with a digital volume meter (Siargo Ltd.). The flow was regularly checked with a Bios Defender calibration unit and considered stable throughout the campaign. In the laboratory, the RM content on the PES after digestion was determined using a Brooks Rand Model III cold vapor atomic fluorescence spectrometer (CVAFS). The method detection limit (MDL) was 5 pg Hg[25]. Details on RM analysis are described in section S2 and a data overview is given in section S3. In total, eight blank membranes were collected from the jars that housed the PES prior to deployment of the new samples. The mean Hg content on PES blanks was 13 ± 8 pg (1σ, n = 8). The limit of detection (LOD) was 25 pg (3σ of blank). The lowest RM on PES was 333 pg, collected from June 4 to June 11, 2019. The blank percentage compared to the median RM was 2% (ranged from 1% to 6%) and all samples were above the LOD.

2.3.2 RMAS membrane total Hg measurements

The RMAS was used to collect RM on CEM and nylon membranes. The sampling procedures for CEM and nylon membranes and their blank treatments were identical. Previous studies showed that nylon membranes did not collect all ambient compounds with the same efficiency as CEMs[19,53], but that the RM chemistry was in good agreement with measurements of anions (e.g., Cl^-, Br^-, NO_3^-)[24], and that RM compounds sorbed to the membrane did not transform during storage and shipment[53]. For RM sampling, ambient air was drawn through 6 sampling ports (n = 3 CEM, n = 3 nylon) at a flow rate of 1.7 ± 0.2 L min^{-1}. The downstream membranes in the two-stage filter holders allowed for the capture of Hg that passed through the upstream membrane. A detailed description of the RMAS can be found in Luippold et al.[24]. Triplicate blank CEM and nylon membranes were collected from the same jars as those that held the sample membranes. CEM and downstream nylon membranes were digested and analyzed using CVAFS following EPA Method 1631, and upstream nylon membranes are thermally desorbed (sections 2.4, S2). The mean of the triplicate CEM blanks, collected weekly at the start of each deployment, was 38 ± 13 pg (1σ, n = 17), and the mean nylon membrane blank Hg content was 14 ± 7 pg (1σ, n = 17). All CEM samples were above the LOD of 38 pg (3σ of blank); the LOD was less than 5% of the median RM (785 pg). Median CEM breakthrough for all samples was 8% (n = 17). The nylon membrane LOD was 20 pg (3σ of blank); the two last samples of the campaign (harvested on July 17 and 24, 2019) were below the LOD. The mean breakthrough on the nylon membrane was 2% (1σ, n = 15), excluding the samples below the LOD.

2.4 RM compounds

Upstream nylon membranes were thermally desorbed to characterize and quantify RM compounds. The thermal desorption profiles for different RM compounds (Section S4) were compared to pure GOM compounds for which profiles have been developed, including HgO, $HgBr_2$, $HgCl_2$, HgN_2O_6,

$HgSO_4$, and elemental Hg, as well as methylmercury chloride directly added to membranes[20,21,36]. Thermal desorption profiles have been used to identify Hg compounds not only in ambient air but in other matrices. Exemplarily, Biester and Scholz[55] developed profiles for solids that have peaks at similar locations as ours for similar compounds.

Individual RM compounds were identified from peak deconvolution of thermal desorption profiles[19,20,24,32]. Each profile was considered to follow a Gaussian distribution (Section S3) and was deconvoluted based on the curve fitting function in MATLAB v. 2018a. Peak temperature ranges were defined for different compounds using an improved calibration system: 80–85 °C for [-O], 90–110 °C for [-Br/Cl], 125–135 °C for [-N], 150–155 °C for [-S], and 180–190 °C for methylmercury (MeHg) or generally organic Hg compounds[24,32]. To quantify the RM compounds on each nylon membrane, the integral of the area beneath each Gaussian peak was calculated ($pg \cdot m^{-3} \cdot °C$). The relative contribution of each RM compound was calculated based on the integrated peak area. The percentage of the compounds was determined by dividing the concentration of the identified compound using thermal desorption data, specifically the area under the curve, by the total amount of RM measured. RM compound contribution collected on each nylon membrane was determined weekly based on the peak deconvolution analysis. For details on the thermal desorption and peak deconvolution procedures, see Luippold et al.[32].

2.5 Back trajectory modeling

The Hybrid Single-Particle Lagrangian Integrated Trajectory model (HYSPLIT, v. 4.2.0), developed by NOAA[56], was driven with 3-hourly meteorological input data from the Global Data Analysis System (GDAS; 1° latitude-longitude 360 by 181 grid) to identify the potential source regions of RM compounds. The model was run in backward mode for 10 days every 2 hours throughout the CEM and nylon membrane sampling periods at Zeppelin (474 m a.s.l.). In total, ~84 backward trajectories were calculated for each sampling period. The spatial (horizontal and vertical) residence time of the air masses were calculated. The back trajectory model results were combined with five major surface categories – land (no snow cover), open water, permanent ice/snow, sea ice, and snow on land, determined using ESRI ArcGIS Pro (v. 10.6) – to provide the time series of percent surface exposure of particles along trajectories. Moreover, the percent of particles along trajectories that reside within the boundary layer (BL) and in the free troposphere (FT) was analyzed. Details on generation of surface maps and back trajectory statistics are given in section S5.

2.6 GOM/RM dry deposition

2.6.1 Dry deposition measurements

Three passive Aerohead samplers were deployed to measure GOM dry deposition[33,34] next to the inlets for the automated and manual RM samplers. GOM was collected on CEM (127 mm diameter, 0.8 μm pore size; Mustang-S, Pall Corporation) on a weekly basis. After each deployment, the three CEM and two non-deployed blanks were collected. The samples were stored in 50 mL centrifuge tubes in

double-zipper bags at -20 °C. In the laboratory, the membranes were digested and analyzed identically to the CEM and nylon from the RMAS. Dry deposition of RM was calculated following Lyman et al. [34]:

$$D = \frac{\left[\frac{S-B}{A}\right]}{T}, \quad (1)$$

where D is the deposition rate in ng m^{-2} h^{-1}, S is the mass of Hg on the membrane (ng), B is the mass of Hg on the method blanks (ng), A is the surface area of the membrane (0.0104 m^2), and T is the deployment duration (h). The mean of all Aerohead CEM blanks was 166 ± 112 pg (1σ, n = 35). The RM dry deposition MDL for a weekly deployment was 0.29 ng m^{-2} h^{-1} (blank + 3σ). Uncertainty in the GOM dry deposition measurements originiates from the fact that we measure deposition on an artificial surface and not on snow, ice or tundra vegetation directly, where GOM can be reduced and subsequently re-emitted to the atmosphere. The surface of the CEM provides physical means for understanding temporal changes of GOM dry deposition[34].

2.6.2 Dry deposition modeling

Weekly dry deposition of RM was estimated in a three step procedure. First, we determined the individual RM compounds ($Hg(OH)_2$, $HgBr_2$/$HgCl_2$, HgN_2O_6, $HgSO_4$, MeHg) using thermal desorption and peak deconvolution procedures (Section 2.4). Second, we calculated the RM compound specific dry deposition velocity using a multi-resistance model[37]. The basic source code of the multi-resistance model was described in Lyman et al.[33] and was subsequently applied by Huang et al.[36]. Here the code was modified according to the description in section S6, and is publicly accessible (https://github.com/JiaoyanHuang/Dry_Depo_multi_res_model). The meteorological model input parameters were derived from hourly ERA5 data, the fifth generation ECMWF atmospheric reanalysis of the global climate[57]. The meteorological data were representative for a 31 km grid covering the area around Zeppelin. Snow depth was determined at two measurement stations representing a lower and upper limit of snow depth in the area. The first station, representing low snow depth, was located on a measurement field just south of the Ny-Ålesund village; the second station, Bayelva, was located about 3 km outside the village and represented the upper limit of snow depth[58]. Third, we multiplied the RM compound specific dry deposition velocities (calculated by the model) with the relative percentage of the RM compound concentrations measured by the Tekran® or from CEM analysis.

2.7 Uncertainty in RM dry deposition modeling

The uncertainty of the modeled RM dry deposition was assessed using the Monte Carlo simulation approach (Crystal Ball®) and is reported as the 95% confidence interval of 10,000 simulations. The probability distributions of the key input parameters for the model was obtained using the "BatchFit" function in Crystal Ball® based on the dataset for each sampling period. Normal distribution and log-normal distribution were chosen for distribution fitting, and the *p* values for the significance levels of the fitted distributions were all < 0.05. The uncertainty analysis, however, does not include the issues of 1) lower sorption efficiency (ca. 50%) of RM on nylon membranes compared to CEMs and 2) that

during peak deconvolution mixed compounds, e.g. $HgBrNO_3$, are not well-defined. In order to minimize these uncertainties, the nylon membranes were not used as a quantitative sorption surface but for RM compound analysis only. Several studies have confirmed, that nylon membranes sorbed Hg-Br and Hg-Cl compounds linearly with increasing concentrations (under ambient and laboratory conditions)[22,53], and these compounds were neither lost nor transformed RM during sampling and storage[53]. However, CEM collected systematically higher concentrations of $HgBr_2$, $HgCl_2$, and a HgO compound[21]. More recent work has demonstrated that the nylon membranes do not effectively collect Hg-N compounds[20]. We are learning incrementally about the use of membrane for identifying the chemistry of the compounds. Thermal desorption and peak deconvolution procedure introduces uncertainty, because there are only a limited number of RM compounds for which calibration profiles can be developed and currently the desorption profiles are broad. However, comparing the chemistry of the compounds to oxidants measured or expected in the air for a variety of locations, as well as ion chromatography measurement of ions on the nylon membranes, supports the RM chemistry observed. For example, in Hawaii halogenated compounds were dominant, while in Nevada adjacent to a high way N-S-O Hg compounds were present, and in a forested area in Maryland organic compounds were measured[24]. This indicates that we are effectively getting at the compounds in general, although we do not know the exact chemistry. More work needs to be done to quantify the chemistry and develop surfaces that are better at retaining compounds.

2.8 Auxiliary variables

Meteorological parameters from Zeppelin, including air temperature, wind speed, wind direction, relative humidity, and atmospheric pressure, were provided with an hourly resolution by NILU. Hourly means of tropospheric O_3 concentrations were measured by NILU using a UV absorption spectrometer (API 400A). Hourly means of particulate matter concentrations ($PM_{2.5}$, PM_{10}, and PM_{total}) were derived from a FIDAS® 200S instrument (Palas GmbH, Germany) operated by Stockholm University (SU). Daily means of particulate and gaseous nitrogen compounds (HNO_3/NO_3^-, NH_4^+/NH_3) were collected on a three stage filter pack and analyzed using a Thermo Scientific Dionex Integrion HPIC System equipped with a Dionex AS9-column[59] and made available by NILU.

3. Results and Discussion

3.1 Quantification of atmospheric Hg using the Tekran® system

The mean GEM ± 1σ concentration measured between March 26 and July 27, 2019 was 1.36 ± 0.4 ng m^{-3} (Figure 1a). During that period, nine distinct AMDEs were identified, with eight observed in April and May and one in early June. The occurence of an AMDE was defined when GEM decreased below 1 ng m^{-3} [41] and the O_3 concentration dropped below the 5th percentile (33 µg m^{-3}). An AMDE starts when the concentration of GEM sharply decreases and ends when GEM increases again to average concentrations. Due to AMDEs, GEM concentrations in the Arctic are typically the lowest in April

and May. From 2000 – 2009[39] and 2011 – 2015[48], 86% and 75%, respectively, of annual observed AMDEs occurred during the April and May time period. Due to the influence of AMDEs during the sampling campaign, the mean GEM concentration during the campaign (1.36 ng m^{-3}) was lower than the annual mean of 1.54 ± 0.3 ng m^{-3} measured between 2000 and 2009[39] and annual means ranging from 1.47 – 1.51 ng m^{-3} between 2011 and 2015[48]. In summer, GEM increases due to re-emission of previously deposited Hg to surfaces and re-emission of surface Arctic Ocean dissolved Hg^0 [60-62].

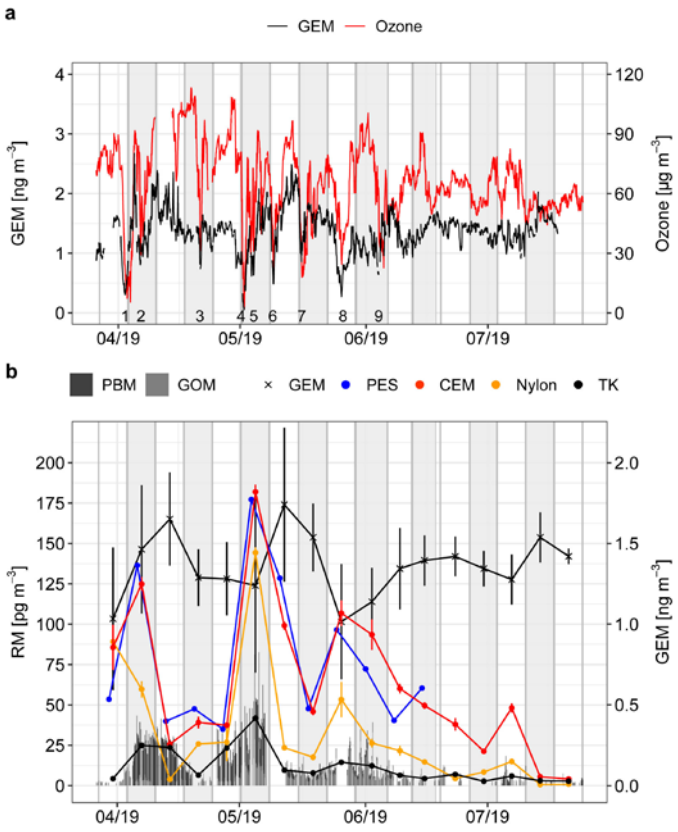

Figure 1: Time series of atmospheric Hg species and O_3 from March 26 to July 27, 2019. (a) GEM (black line) and O_3 (red line) concentrations are displayed as hourly means. AMDEs are indicated with numbers 1 to 9. (b) Mean concentration of GEM (black cross), RM on PES (blue dots), RM on CEM (red dots), and RM on nylon membranes (orange dots). RM from Tekran® (TK) measurements (black dots), as PBM and GOM measurements (gray bars), are also displayed. Error bars represent 1σ and are indicated where n ≥ 3. PES, CEM, and nylon membranes were deployed for one week. Sampling periods for CEM and nylon membranes are indicated with alternate white and gray backgrounds. The weekly PES sampling was offset from CEM and nylon membrane by one day.

Automated Tekran® measurements of RM (GOM+PBM) for the whole sampling campaign were in the range of 2.6 – 13.1 pg m^{-3} for GOM and 2.1 – 29.9 pg m^{-3} for PBM (10^{th} and 90^{th} percentiles). The mean Tekran® RM concentration (RM_{TK}) was 14.6 ± 12.7 pg m^{-3}, and the values spanned from below the MDL to 82.6 pg m^{-3} (Figure 1b). During AMDEs, GOM and PBM concentrations were 9.6 and 20.5 pg m^{-3}, on average, and elevated by 42% and 54%, respectively, compared to the entire campaign average. These values were at the lower end compared to those measured at Zeppelin during AMDEs in 2003[41] and in 2007-2008[47]. Overall, RM_{TK} was < 43.5 pg m^{-3} (90^{th} percentile) during AMDEs and lower (< 30.8 pg m^{-3}, 90^{th} percentile) during the entire campaign.

3.2 Quantification of RM using manual methods

Mean RM concentration sampled on CEM (RM_{CEM}) was 63 ± 45 pg m^{-3} (Section S3). The highest concentrations were found between May 1 and May 8 (182 pg m^{-3}) and lowest at the end of the campaign from July 17 to July 24 (4 pg m^{-3}). The large variation among samples was due to the occurrence of AMDEs until the beginning of June (Figure 1b). Thereafter, RM_{CEM} tended to decrease, with one exception from July 3 to July 10 when RM_{CEM} was 48 pg m^{-3}. The RM concentration on PES (RM_{PES}) was sampled until June 18, 2019 and was similar to RM_{CEM} even though the PES were replaced one day in advance compared to CEM (slope = 0.91, r^2 = 0.86; Figure S1a). The mean RM_{PES} was 78 ± 46 pg m^{-3}, similar to mean RM_{CEM} concentrations for the same period to within 2% (March 26 – June 18). The good agreement between the CEM and PES materials was previously demonstrated by Dunham-Cheatham et al.[53], showing no significant difference between the two materials ($\alpha = 0.05$). In concert with that study, the nylon membranes in this study were less efficient at capturing RM.

The mean RM concentration on nylon membranes (RM_{Nylon}) was 32 ± 37 pg m^{-3}. The nylon membrane recovery was 50% (range from 12 to 104%) of the RM sorbed on CEM (Figure 1b). The lower RM content on nylon membranes was likely due to the different sorption efficiency of varying RM compounds to this material[19,20,24,36]. Despite the difference in captured RM, the relationship between RM_{CEM} and RM_{Nylon} was fairly constant (r^2 = 0.75, $p < 0.05$, section S3). This supports the conclusions from previous studies that nylon membranes are not suitable for quantitative RM concentrations, but are suitable for thermal desorption analysis to identify RM compounds[19,53].

Weekly mean RM_{CEM} and RM_{PES} were up to 19 times and 22 times higher compared to RM_{TK}, respectively (Figure S1b). On average, the RM_{CEM} was 5.3 times and RM_{PES} 5.2 times higher than RM_{TK} based on weekly averages (11.8 ± 10.4 pg m^{-3}). Tekran® RM measurements were calculated as the sum of GOM and PBM concentrations and the amount of Hg released during the three 5-min flush cycles ($flush_{TK1-3}$). The discrepancy between RM on membranes and RM_{TK} agrees with recently performed comparisons, where RM on membranes was 2 to 13 times greater[17,18,20-22]. However, we would like to point out that the impactor on the Tekran® removes particles with aerodynamic diameters larger than 2.5 µm while the membrane-based systems might also capture particles > 2.5 µm. The mean $PM_{2.5}$ concentration (0.97 µg m^{-3}) was only 30% of the total mean PM concentration (3.29 µg m^{-3}) measured during our campaign. Thus, RM_{TK} tend to be lower compared to membrane-based systems due to the lower efficiency of GOM collection[63] and due to the exclusion of large PBM (> 2.5 µm) from analysis. More multi-season RM_{CEM} and RM_{PES} timeseries at multiple Arctic sites are necessary to derive robust correlations with automated measurements and to potentially correct previous Tekran® RM data.

3.3 Compounds of RM

Thermal desorption and peak deconvolution revealed the composition of RM species that were retained on the nylon membranes (section S4). The weekly mean RM_{Nylon} ranged from 1 to 144 pg m^{-3}

(Figure 2a). The dominant RM compounds sampled over the course of the campaign were Hg-Br/Cl and Hg-N, that accounted for 51% and 45%, respectively, of the total RM on nylon membranes (Figure 2b). Organic-based Hg compounds (e.g. MeHg) contributed 2% to the overall RM concentration. Sulfur compounds (Hg-S) accounted also for 2% while the contribution of oxide compounds (HgO) was < 1%. The relative contribution of the RM compounds was calculated each week throughout the campaign (Figure 2c). The Hg–Br/Cl compounds indicate reactions of GEM with halogens (Cl, Cl_2, Br, Br_2) within the atmospheric BL[7], where Br• is regarded as one of the primary first-step atmospheric oxidants to produce RM intermediates such as $Hg^{I}Br$[11,64]. The occurrence of Hg–N compounds depends on several different factors, such as N emission sources or atmospheric redox processes occurring between the source and receptor site[65-67]. Atmospheric NO_2 radicals are also considered to be the dominant second-step oxidant transforming $Hg^{I}Br$ to $Hg^{II}BrONO$ in the free troposphere[64,68]. During the first sampling deployment week, RM was composed of 34% Hg–Br/Cl and 58% Hg–N compounds, but in contrast, during week two, 68% Hg–Br/Cl and 32% Hg–N were detected. During week 6, when two AMDEs occurred and the largest RM concentrations were measured (182 pg m^{-3}), Hg–Br/Cl and Hg–N contributed similar parts to total RM (58% and 42%, respectively). During weeks seven and eight, the dominant RM compound on the nylon membranes changed from Hg–N (70%) to Hg–Br/Cl (89%). To explain differences in chemical composition, we investigated the role of air mass exposure on the dominant RM compounds, Hg–Br/Cl (51%) and Hg–N (45%), along the air mass back trajectory.

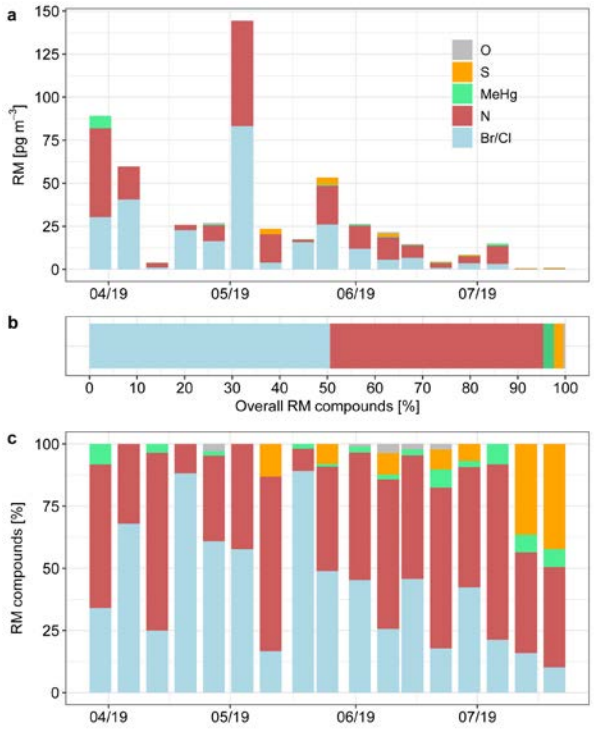

Figure 2: RM compounds determined from March 27 until July 24, 2019. (a) The RM concentration on the nylon membrane from the RMAS for a mixture of RM compounds identified by thermal desorption and peak deconvolution. The frequency distribution of RM compounds, in %, is given (b) for the entire campaign (mean) and (c) for each sampling event.

3.4 Origin of RM

To investigate if atmospheric conditions influence the RM compounds, the relationship between the trajectories within the BL and in the FT was analyzed. The percentage of time the trajectories arriving at Zeppelin resided in the BL ranged from 7% to 50% (Figure 3a). There was a significant correlation between the percentage of time the trajectories were within the BL and the determined percentage of Hg–Br/Cl compounds ($r^2 = 0.4$, $p < 0.05$). The relationship became even stronger during periods when AMDEs occurred ($r^2 = 0.7$, $p < 0.05$) (Figure 3b). During the same period, Hg–N compounds occurred more frequently when the advected air mass originated from the FT ($r^2 = 0.7$, $p < 0.05$) (Figure 3c). This indicates that air masses enriched in Hg–Br/Cl were in contact with the surface for longer periods compared to air masses enriched in Hg–N, that were originating predominantly in the FT.

Air masses arriving at Zeppelin were mainly exposed to sea ice and open water (Figure 3d). The RM concentrations increased when air masses were exposed to sea ice ($r^2 = 0.32$, $p < 0.05$) or land covered by snow ($r^2 = 0.36$, $p < 0.05$) (Figure 3e). Lower RM concentrations were measured when air masses were exposed to open water ($r^2 = 0.43$, $p < 0.05$) (Figure 3f). The positive relationship between Hg–BrCl and the time the air mass passed over sea ice ($p = 0.06$, Figure S4) further corroborates that sea ice and snow on sea ice are the main source of reactive halogen species in the Arctic that oxidize GEM. This can occur via one of two mechanisms, activation from snow on sea ice (surface snow source)[69] or lofted salty snow particles that form sea salt aerosols within the BL (blowing snow particle source)[70,71].Though Hg–Br and Hg–Cl compounds are indistinguishable with our methods, all reactive halogen species in the atmosphere are produced from similar sources, i.e., snow on sea ice and BL aerosols[72-74]. In the atmosphere, both Br• and Cl• react with O_3 to form halogen oxides[75,76]; both halogen radicals and halogen oxides lead to the oxidation of GEM to RM[10].

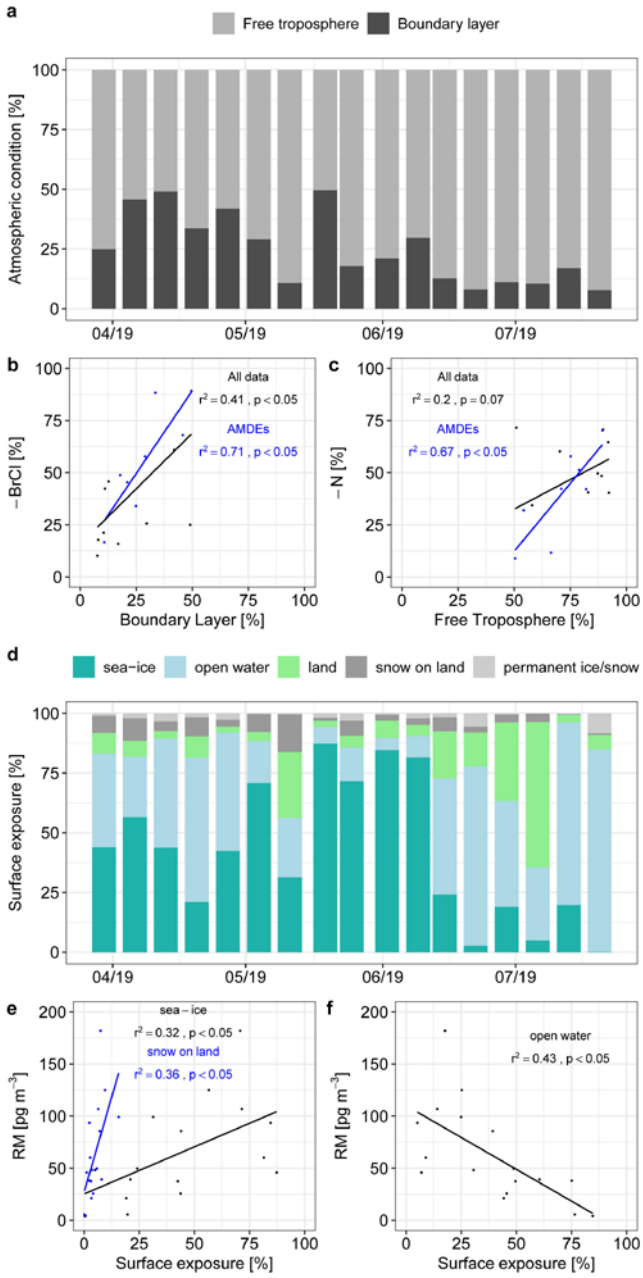

Figure 3: HYSPLIT simulation of air mass trajectory residence time in the atmosphere and exposure to surfaces. (a) Percentage of time the trajectories were in the boundary layer (BL) and free troposphere (FT) for each of the 17 deployment periods. Linear correlation during the entire campaign and during weeks when AMDEs occurred (b) between Hg-Br/Cl and residence time in the BL and (c) Hg-N and residence time in the FT. (d) Surface exposure of trajectories to the 5 major surface categories: sea ice, open water, land (no snow), snow covered land, and permanent ice and snow. Linear correlation between (e) RM_{CEM} and exposure to sea ice and snow covered land, and between (f) RM_{CEM} and exposure to open water.

A weak positive relationship between Hg–N and the time the air mass passed over land without snow cover (r^2 = 0.2, p = 0.06, Figure S4) indicated an anthropogenic source of N compounds (i.e. NO_2) from more densely populated areas further south, or more specifically, springtime transport of plumes from Asian industries or Siberian wildfires[77]. Emitted NO_2 leads to enhanced GEM oxidation and increased Hg-N concentrations downwind. Though more data are required (multi-seasonal sampling) to establish significant relationships between RM compounds and exposure time of air masses to

different surface types, our conclusions are well illustrated by comparing surface exposure during weeks seven and eight. A maximum of Hg–N compounds was measured during week 7 (70% of total RM), when exposure time of air masses over land (43%) and the residence time in the FT (89%) were long. Back trajectory analysis indicated that the air moved mainly from Fennoscandia (17%) and Siberia (74%) over the eastern Arctic Ocean to Zeppelin (Figure S5g). The Siberian air mass originated from areas where wildfires were ubiquitous between May 8 and May 15, 2019 (https://earthdata.nasa.gov/earth-observation-data/near-real-time/firms). The mean BL height measured along the air mass trajectories was 277 m a.s.l and was elevated compared to week 8 (87 m a.s.l). In week 8, Hg–Br/Cl was the dominant RM compound (89%) and air masses passed predominantly over sea ice (87%) from areas east of Zemlya Georga and northwest of Svalbard to Zeppelin (Figure S5h). The residence time of the air mass in the BL was 50%, which corresponded to the longest residence time in the BL among all weeks of sampling (Figure 3a). Thus, the comparatively long residence time of air masses within the BL over the sea ice-covered Arctic Ocean constituted the main source region of Hg–Br/Cl arriving at Zeppelin.

3.5 Dry deposition measurements and modeling

Mean local GOM dry deposition at Zeppelin measured by Aerohead samplers was 0.35 ng m^{-2} h^{-1}, and weekly averages ranged from below the MDL to 1.47 ng m^{-2} h^{-1} (Figure 4). Measurements of GOM dry deposition in 9 out of 17 weeks were above the MDL (0.29 ng m^{-2} h^{-1}). The cumulative Aerohead GOM dry deposition measured from March 27 to July 24, 2019 was 1 µg m^{-2}, with a 95% confidence interval ranging from 0.74 to 1.25 µg m^{-2} (Figure 4). Dry deposition of GOM measured by Aerohead samplers was negligible (< 0.1% of the cumulative flux) during the last 5 weeks of measurements (June 19 to July 27, 2019). During weeks 3 and 4, there was less than 1 pg GOM measured on the Aerohead CEM, in contrast to 795 pg analyzed on the CEMs from RMAS indicating the importance of particulate-bound Hg. During weeks 5 and 9, measured GOM dry deposition exceeded the modeled RM dry deposition by 38% and 43%, respectively. A comparison of meteorological and chemical variables during these weeks with the preceding and following weeks indicated no unusual conditions. It could be a compound was present that was sticking to the open-faced membranes in the Aeroheads, but not making its way into the filter packs holding membranes in the RMAS or the compound had a higher deposition velocity than other compounds. This would be true for HgO that once formed is thought to become a particle and rapidly deposit to surfaces[78]. Thus, understanding reactions forming and the chemistry of compounds of GOM/RM is greatly needed.

The cumulative modeled dry deposition of RM, based on RM compound-specific dry deposition velocities and RM_{TK}, was 0.33 µg m^{-2} with a 95% confidence interval ranging from 0.23 to 0.50 µg m^{-2} (Figure 4). The modeled flux was one-third of the measured flux. The average RM dry deposition velocities of $Hg(OH)_2$, $HgBr_2/HgCl_2$, HgN_2O_6, $HgSO_4$, MeHg were very similar and differed by less than 5% during each sampling week (Table S6). The dominant RM compounds $HgBr_2/HgCl_2$ and

HgN_2O_6 both exhibited a mean deposition velocity of 0.28 ± 0.10 cm s^{-1} over the course of the campaign. The weekly mean RM deposition velocities ranged from 0.12 cm s^{-1} (week 15) to 0.48 cm s^{-1} (week 10). The mean deposition velocity of all RM compounds was 0.32 ± 0.09 cm s^{-1} when the area around Zeppelin was covered by snow, and 0.21 ± 0.08 cm s^{-1} during the last five weeks of measurements when snowmelt had occurred (June 17, 2019).

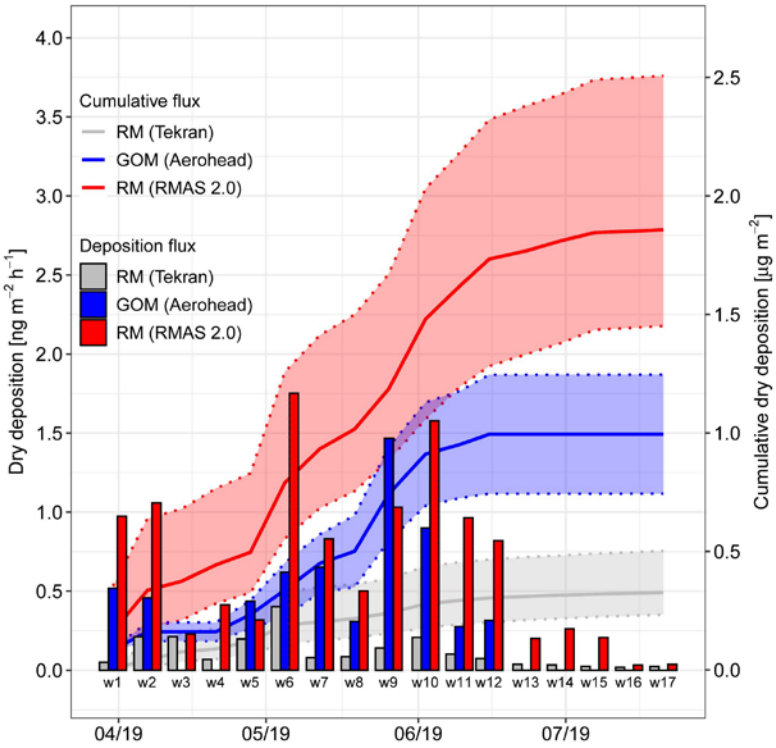

Figure 4: Measured GOM and modeled RM dry deposition for the entire sampling period. Weekly GOM dry deposition calculated based on the Aerohead system (measured) and RM dry deposition estimated based on the Tekran® and RMAS systems using RM compound-specific dry deposition velocities (modeled). The cumulative flux over the entire sampling campaign (lines) and associated uncertainties (shaded area, 95% confidence interval) are given.

The modeled cumulative dry deposition based on RM_{CEM} was 1.86 µg m^{-2} with a 95% confidence interval ranging from 1.45 to 2.50 µg m^{-2} (Figure 4). Thus, RM dry deposition was 5.6 times larger compared to estimates using Tekran® data (Table S7). The discrepancy between the measured (Aerohead) and the modeled (RMAS) cumulative dry deposition, a factor of 1.9, was due to the Aerohead sampling GOM, while PBM adsorbs negligibly to the down-facing surrogate surface due to gravity[22,34-36,79-81]. The inconsistency during weeks 1, 2, and 6 could accordingly be explained by elevated concentrations of particulate matter (PM_{total}), indicating that PBM dominated RM dry deposition during these weeks (Figure S2). The inconsistency in weeks 10, 11 and 12, however, was likely associated with elevated RM dry deposition velocities (0.47 cm s^{-1}), given the low PBM concentrations, as compared to the other weeks (0.25 cm s^{-1}) that are not reproduced by the Aerohead measurements. It is likely that Hg–N RM compounds were advected on particles, especially during weeks 1 and 6 when the absolute amount of Hg–N RM compounds was elevated (Figure 2a). During the entire campaign, though, the ammonium (NH_4^+) and nitrate (NO_3^-) aerosol concentration was at least three orders of magnitude higher compared to the concentrations of Hg–N compounds. This

indicates that RM production and transformation of Hg–N compounds was not directly linked to advection of particulate nitrogen compounds, which is consistent with a predominant gas-phase oxidation of RM precursor by NO_2 in the FT[64].

3.6 Implications

Arctic RM concentrations analyzed on CEM and PES were higher than Tekran® RM during all weeks of measurements. That the Tekran® system significantly underestimated RM concentrations in the Arctic was surprising since one would expect that most of the RM would be Br and Cl compounds and given the efficiency of the denuder the KCl denuder it should be 1.2 to 1.3 times lower as demonstrated in Huang et al.,[21]. But Huang et al. [21]'s experiments were done in clean air whereas the measurements in the Arctic were of ambient air, indicating the impact of some aspect atmospheric chemistry (e.g. O_3) on retention of GOM compounds.The difference between RM concentrations was large during the AMDE season (mainly April and May) and became small when the RM concentrations decreased in the summer. In general, RM_{TK} showed a significant, but not strong, correlation ($r^2 < 0.6$) with RM_{CEM} and RM_{PES}. Bias in denuder-based Tekran® quantification of GOM could not be corrected, as was suggested for the Pic du Midi high-altidute site in the Pyrenees, France[25]. The bias in Arctic RM concentration measurements between manual and automated methods must be addressed not only during AMDEs but with multi-seasonal sampling campaigns at sites such as Alert in Canada, where Tekran® systems are also operated year-round.

RM compound-specific deposition velocity estimates provide the way for more accurate RM dry deposition estimates. However, as stated in Gustin et al.[63], the determination of RM compounds could be improved by: 1) using a new thermal desorption surface, because the nylon membranes underestimate RM concentrations (by 50% in this study); and 2) identifying the exact chemistry of RM compounds by developing a mass spectrometry method.

The RM dry deposition model revealed higher fluxes when using the RMAS data compared to Tekran® data, suggesting a 5.6 times larger input of RM to Arctic ecosystems. In the Ny-Ålesund area, RM dry deposition (1.9 µg m^{-2} from March 27 to July 24, 2019) was the dominant Hg deposition pathway, exceeding mean annual wet deposition ranging from 0.8 to 1.7 µg m^{-2} yr^{-1} measured between 2012 and 2015[82].

If we accept the assumption that dry deposition measurements made by the Aerohead system are accurate for GOM and measurements performed with RMAS are accurate for RM, our results demonstrate that RM bound to particles constituted 46% of the deposited Hg; this also assumes that RM dry deposition occurs homogeneously and independently of different boundary layer conditions at Zeppelin. In fact, large particles > $PM_{2.5}$ (not analyzed by the Tekran®) contributed 70% to the total PM concentration (Figure S2). This indicates that a dominant portion of the RM was associated with large particles (> $PM_{2.5}$), likely marine aerosols. Our study showed that RM dry deposition estimates

during the 2019 AMDE season at Zeppelin, and potentially elsewhere in the Arctic, were likely higher than previously assumed and reported. This has implications for the amount of Hg cycling between the atmosphere and Arctic ecosystems.

Associated content (Supporting Information)

The Supporting Information (SI) is available free of charge on the ACS publication website. The SI is structured in six different sections (S1 – S6). We provide details on automated (S1) and manual (S2) RM sampling and analysis as well as an overview of the measured RM concentrations (S3). The thermal desorption procedure is described and profiles displayed (S4). Back trajectory modeling is detailed in S5 and supplementary information about dry deposition modeling is given in S6.

Author information (corresponding author)

Stefan Osterwalder - Institute of Agricultural Sciences, ETH Zurich, Universitätsstrasse 2, 8092 Zurich, Switzerland; orcid.org/0000-0001-8775-0813; Phone: +41 76 477 35 89; Email: stefan.osterwalder@usys.ethz.ch

Financial sources

This research was funded by the French Polar Institute IPEV (Programme 1207 MESSI), the EC H2020 ERA-PLANET (grant no. 689443) iGOSP and iCUPE programmes. The project also received funding from the Swiss National Science Foundation (SNSF) project P400P2_180796 and the NSF project 1700711.

Acknowledgements

We thank the following persons for assistance in the field and laboratory: Laure Laffont from GET, Ove Hermansen and Are Bäcklund from NILU, Christelle Guesnon from NPI and all personnel from IPEV and Alfred Wegener Institute (AWI) for Polar and Marine Research. We acknowledge Hans-Werner Jacobi from Université Grenoble Alpes, Julia Boike, Christian Lehr and Siegrid Debatin from AWI for providing snow depth data. We are grateful to Paul Zieger from SU for providing PM data from Zeppelin. We would like to thank Wenche Aas (NILU) for making data on particulate and gaseous nitrogen compounds available. The student assistants from the University of Nevada, Reno lab are acknowledged for their support with membrane digestion and analysis. The authors thank 3 anonymous reviewers for their comments.

Data availability

RM concentration data are given in the Supporting Information. A detailed model description is provided in https://github.com/JiaoyanHuang/Dry_Depo_multi_res_model. Raw data on thermal desorption and peak deconvolution procedures or from back trajectory modeling are available on request.

References

(1) AMAP Assessment 2011: Mercury in the Arctic., Arctic Monitoring and Assessment Programme (AMAP), Oslo, Norway., **2011**.

(2) Douglas, T.A., Loseto, L.L., Macdonald, R.W., Outridge, P., Dommergue, A., Poulain, A., Amyot, M., Barkay, T., Berg, T., Chételat, J., Constant, P., Evans, M., Ferrari, C., Gantner, N., Johnson, M.S., Kirk, J., Kroer, N., Larose, C., Lean, D., Nielsen, T.G., Poissant, L., Rognerud, S., Skov, H., Sørensen, S., Wang, F., Wilson, S. Zdanowicz, C.M. The fate of mercury in Arctic terrestrial and aquatic ecosystems, a review. *Environ. Chem.* **2012**, 9, 321-355. http://dx.doi.org/10.1071/EN11140

(3) UNEP Minamata Convention on Mercury: Text and Annexes. UNEP Chemicals Branch, Geneva, Switzerland, **2013**. http://www.mercuryconvention.org (last access: 12. April 2021).

(4) Soerensen, A.L., Jacob, D.J., Schartup, A.T., Fisher, J.A., Lehnherr, I., Louis, V.L.S., Heimbürger, L.-E., Sonke, J.E., Krabbenhoft, D.P., Sunderland, E.M. A mass budget for mercury and methylmercury in the Arctic Ocean. *Glob. Biogeochem. Cycles* **2016**, 30, 560–575. https://doi.org/10.1002/2015GB005280

(5) Dastoor, A.P. and Durnford, D.A. Arctic Ocean: Is It a Sink or a Source of Atmospheric Mercury? *Environ. Sci. Technol.* **2014**, 48, 1707-1717. https://doi.org/10.1021/es404473e

(6) Schroeder, W.H., Anlauf, K.G., Barrie, L.A., Lu, J.Y., Steffen, A., Schneeberger, D.R., Berg, T. Arctic springtime depletion of mercury. *Nature* **1998**, 394, 331–332. https://doi.org/10.1038/28530

(7) Ariya, P.A., Dastroor, A.P., Amyot, M., Schroeder, W.H., Barrie, L., Anlauf, K., Raofie, F., Ryzhkov, A., Davignon, D., Lalonde, J., Steffen, A. The Arctic: a sink for mercury. *Tellus B: Chemical and Physical Meteorology* **2004**, 56, 397–403. https://doi.org/10.3402/tellusb.v56i5.16458

(8) Skov, H., Christensen, J. H., Goodsite, M. E., Heidam, N. Z., Jensen, B., Wåhlin, P., Geernaert, G. Fate of elemental mercury in the arctic during atmospheric mercury depletion episodes and the load of atmospheric mercury to the arctic. *Environ. Sci. Technol.* **2004**, 38, 2373–2382. https://doi.org/10.1021/es030080h

(9) Lindberg, S. E., Brooks, S., Lin, C.-J., Scott, K. J., Landis, M. S., Stevens, R. K., Goodsite,M. E., Richter, A. Dynamic oxidation of gaseous mercury in the arctic troposphere at polar sunrise. *Environ. Sci. Technol.* **2002**, 36, 1245–1256. https://doi.org/10.1021/es0111941

(10) Steffen, A., T. Douglas, M. Amyot, P. Ariya, K. Aspmo, T. Berg, J. Bottenheim, S. Brooks, F. Cobbett, A. Dastoor, A. Dommergue, R. Ebinghaus, C. Ferrari, K. Gardfeldt, M.E. Goodsite, D. Lean, A.J. Poulain, C. Scherz, H. Skov, J. Sommar, Temme, C. A synthesis of atmospheric mercury depletion event chemistry in the atmosphere and snow. *Atmos. Chem. and Phys*. **2008**, 8, 1445–1482. https://doi.org/10.5194/acp-8-1445-2008

(11) Wang, S., McNamara, S.M., Moore, C.W., Obrist, D., Steffen, A., Shepson, P.B., Staebler, R.M., Raso, A.R.W., Pratt, K.A. Direct detection of atmospheric atomic bromine leading to mercury and ozone depletion. *PNAS* **2019**, 116, 14479–14484. https://doi.org/10.1073/pnas.1900613116

(12) Obrist, D., Agnan, Y., Jiskra, M., Olson, C.L., Colegrove, D.P., Hueber, J., Moore, C.W., Sonke,

J.E., Helmig, D. Tundra uptake of atmospheric elemental mercury drives Arctic mercury pollution. *Nature* **2017**, 547, 201–204. https://www.nature.com/articles/nature22997

(13) Dommergue, A., Larose, C., Faïn, X., Clarisse, O., Foucher, D., Hintelmann, H., Schneider, D., Ferrari, C.P. Deposition of Mercury Species in the Ny-Ålesund Area (79°N) and Their Transfer during Snowmelt. *Environ. Sci. Technol.* **2010**, 44, 901–907. https://doi.org/10.1021/es902579m

(14) Steffen, A., Bottenheim, J., Cole, A., Ebinghaus, R., Lawson, G., Leaitch, W. R. Atmospheric mercury speciation and mercury in snow over time at Alert, Canada, *Atmos. Chem. Phys.* **2014**, 14, 2219–2231. https://doi:10.5194/acp-14-2219-2014

(15) Kamp, J., Skov, H., Jensen, B., Sørensen, L.L. Fluxes of gaseous elemental mercury (GEM) in the High Arctic during atmospheric mercury depletion events (AMDEs). *Atmos. Chem. Phys.* **2018**, 18, 6923–6938. https://doi.org/10.5194/acp-18-6923-2018

(16) Jiskra, M., Sonke, J.E., Agnan, Y., Helmig, D., Obrist, D. Insights from mercury stable isotopes on terrestrial–atmosphere exchange of Hg(0) in the Arctic tundra. *Biogeosciences* **2019**, 16, 4051–4064. https://doi.org/10.5194/bg-16-4051-2019

(17) Gustin, M. S.; Huang, J.; Miller, M. B.; Peterson, C.; Jaffe, D. A.; Ambrose, J.; Finley, B. D.; Lyman, S. N.; Call, K.; Talbot, R.; Feddersen, D.; Mao, H.; Lindberg, S. E. Do We Understand What the Mercury Speciation Instruments Are Actually Measuring? Results of RAMIX. *Environ. Sci. Technol.* **2013**, 47, 7295−7306.

(18) Gustin, M.S., Amos, H.M., Huang, J., Miller, M.B., Heidecorn, K. Measuring and modeling mercury in the atmosphere: a critical review. *Atmos. Chem. Phys.* **2015**, 15, 5697–5713. https://doi.org/10.5194/acp-15-5697-2015

(19) Gustin, M.S., Dunham-Cheatham, S.M., Zhang, L. Comparison of 4 Methods for Measurement of Reactive, Gaseous Oxidized, and Particulate Bound Mercury. *Environ. Sci. Technol.* **2019**, 53, 14489–14495. https://doi.org/10.1021/acs.est.9b04648

(20) Gustin, M.S., Dunham-Cheatham, S.M., Zhang, L., Lyman, S., Choma, N., Castro, M. Use of Membranes and Detailed HYSPLIT Analyses to Understand Atmospheric Particulate, Gaseous Oxidized, and Reactive Mercury Chemistry. *Environ. Sci. Technol.* **2021a**, 55, 893–901. https://doi.org/10.1021/acs.est.0c07876

(21) Huang, J.; Miller, M. B.; Weiss-Penzias, P.; Gustin, M. S. Comparison of Gaseous Oxidized Hg Measured by KCl-Coated Denuders, and Nylon and Cation Exchange Membranes. *Environ. Sci. Technol.* **2013**, 47, 7307−7316. https://doi.org/10.1021/es4012349

(22) Huang, J., Miller, M.B., Edgerton, E., Gustin, M.S. Use of criteria pollutants, active and passive mercury sampling, and receptor modeling to understand the chemical forms of gaseous oxidized mercury in Florida. *Atmos. Chem. Phys. Discuss.* **2015**, 12069–12105. https://doi.org/10.5194/acpd-15-12069-2015

(23) McClure, C.D., Jaffe, D.A., Edgerton, E.S. Evaluation of the KCl Denuder Method for Gaseous Oxidized Mercury using HgBr2 at an In-Service AMNet Site. *Environ. Sci. Technol.* **2014**, 48,

552 11437–11444. https://doi.org/10.1021/es502545k

553 (24) Luippold, A., Gustin, M.S., Dunham-Cheatham, S.M., Castro, M., Luke, W., Lyman, S., Zhang, L.
554 Use of Multiple Lines of Evidence to Understand Reactive Mercury Concentrations and Chemistry in
555 Hawai'i, Nevada, Maryland, and Utah, USA. *Environ. Sci. Technol.* **2020a**, 54, 7922–7931.
556 https://doi.org/10.1021/acs.est.0c02283

557 (25) Marusczak, N., Sonke, J.E., Fu, X., Jiskra, M. Tropospheric GOM at the Pic du Midi Observatory –
558 correcting bias in denuder based observations. *Environ. Sci. Technol.* **2017**, 51, 863–869.
559 https://doi.org/10.1021/acs.est.6b04999

560 (26) Lynam, M.M., and Keeler, G.J. Artifacts associated with the measurement of particulate mercury in
561 an urban environment: The influence of elevated ozone concentrations. *Atmospheric Environ.* **2005**,
562 39, 3081–3088. http://dx.doi.org/10.1016/j.atmosenv.2005.01.036

563 (27) Malcolm, E.G., and Keeler, G.J.: Evidence for a sampling artifact for particulate-phase mercury in
564 the marine atmosphere, *Atmospheric Environ.* **2007**, 41, 3352–3359.
565 https://doi.org/10.1016/j.atmosenv.2006.12.024

566 (28) Rutter, A.P., Hanford, K.L., Zwers, J.T., Perillo-Nicholas, A.L. Evaluation of an offline method for
567 the analysis of atmospheric reactive gaseous mercury and particulate mercury. *J. Air Waste Manag.*
568 *Assoc*. **2008**, 58, 377–383. https://doi.org/10.3155/1047-3289.58.3.377

569 (29) Kos, G., Ryzhkov, A., Dastoor, A., Narayan, J., Steffen, A., Ariya, P. A., Zhang, L. Evaluation of
570 discrepancy between measured and modelled oxidized mercury species, *Atmos. Chem. Phys.* **2013**,
571 13, 4839–4863. https://doi.org/10.5194/acp-13-4839-2013

572 (30) Talbot, R., Mao, H., Feddersen, D., Smith, M., Kim, S.Y., Sive, B., Haase, K., Ambrose, J., Zhou,
573 Y., Russo, R. Comparison of Particulate Mercury Measured with Manual and Automated Methods.
574 *Atmosphere* **2011**, 2, 1–20. https://doi.org/10.3390/atmos2010001

575 (31) Feddersen, D.M., Talbot, R., Mao, H., Sive, B.C. Size distribution of particulate mercury in marine
576 and coastal atmospheres. *Atmos. Chem. Phys.* **2012**, 12, 10899–10909. https://doi.org/10.5194/acp-
577 12-10899-2012

578 (32) Luippold, A., Gustin, M.S., Dunham-Cheatham, S.M., Zhang, L. Improvement of quantification and
579 identification of atmospheric reactive mercury. *Atmospheric Environ*. **2020b**, 224, 117307.
580 https://doi.org/10.1016/j.atmosenv.2020.117307

581 (33) Lyman, S.N., Gustin, M.S., Prestbo, E.M., Marsik, F.J. Estimation of Dry Deposition of Atmospheric
582 Mercury in Nevada by Direct and Indirect Methods. *Environ. Sci. Technol.* **2007**, 41, 1970–1976.
583 https://doi.org/10.1021/es062323m

584 (34) Lyman, S.N., Gustin, M.S., Prestbo, E.M., Kilner, P.I., Edgerton, E., Hartsell, B. Testing and
585 Application of Surrogate Surfaces for Understanding Potential Gaseous Oxidized Mercury Dry
586 Deposition. *Environ. Sci. Technol.* **2009**, 43, 6235–6241. https://doi.org/10.1021/es901192e

587 (35) Gustin, M.S, Weiss-Penzias, P.S., Peterson, C. Investigating sources of gaseous oxidized mercury in
588 dry deposition at three sites across Florida, USA. *Atmos. Chem. Phys.* **2012**, 12, 9201–9219.

https://doi.org/10.5194/acp-12-9201-2012

(36) Huang, J., Miller, M.B., Edgerton, E., Gustin, M.S. Deciphering potential chemical compounds of gaseous oxidized mercury in Florida, USA. *Atmos. Chem. Phys.* **2017**, 17, 1689−1698. https://doi.org/10.5194/acp-17-1689-2017

(37) Zhang, L., Brook, J.R., Vet, R. A revised parameterization for gaseous dry deposition in air-quality models. *Atmos. Chem. Phys.* **2003**, 3, 2067–2082. https://doi.org/10.5194/acp-3-2067-2003

(38) Berg, T., Bartnicki, J., Munthe, J., Lattila, H., Hrehoruk, J., Mazur, A. Atmospheric mercury species in the European Arctic: Measurements and modelling. *Atmospheric Environ.* **2001**, 35, 2569–2582. https://doi.org/10.1016/S1352-2310(00)00434-9

(39) Berg, T., Pfaffhuber, K.A., Cole, A.S., Engelsen, O., Steffen, A.. Ten-year trends in atmospheric mercury concentrations, meteorological effects and climate variables at Zeppelin, Ny-Ålesund. *Atmos. Chem. Phys.* **2013**, 13, 6575–6586. https://doi.org/10.5194/acp-13-6575-2013

(40) Berg, T., Sekkesæter, S., Steinnes, E., Valdal, A.-K., Wibetoe, G. Springtime depletion of mercury in the European Arctic as observed at Svalbard. *Sci. Total Environ.* **2003**, Pathways and processes of mercury in the environment. Selected papers presented at the sixth International Conference on Mercury as Global Pollutant, Minamata, Japan, Oct. 15-19, 2001 304, 43–51. https://doi.org/10.1016/S0048-9697(02)00555-7

(41) Aspmo, K., Gauchard, P.-A., Steffen, A., Temme, C., Berg, T., Bahlmann, E., Banic, C., Dommergue, A., Ebinghaus, R., Ferrari, C., Pirrone, N., Sprovieri, F., Wibetoe, G. Measurements of atmospheric mercury species during an international study of mercury depletion events at Ny-Ålesund, Svalbard, spring 2003. How reproducible are our present methods? *Atmospheric Environ.* **2005**, 39, 7607–7619. https://doi.org/10.1016/j.atmosenv.2005.07.065

(42) Gauchard, P.-A., Aspmo, K., Temme, C., Steffen, A., Ferrari, C., Berg, T., Ström, J., Kaleschke, L., Dommergue, A., Bahlmann, E., Magand, O., Planchon, F., Ebinghaus, R., Banic, C., Nagorski, S., Baussand, P., Boutron, C. Study of the origin of atmospheric mercury depletion events recorded in Ny-Ålesund, Svalbard, spring 2003. *Atmospheric Environ.* **2005**, 39, 7620–7632. https://doi.org/10.1016/j.atmosenv.2005.08.010

(43) Sprovieri, F., Pirrone, N., Landis, M.S., Stevens, R.K. Oxidation of Gaseous Elemental Mercury to Gaseous Divalent Mercury during 2003 Polar Sunrise at Ny-Ålesund. *Environ. Sci. Technol.* **2005a**, 39, 9156–9165, https:// doi.org/10.1021/es050965o

(44) Sprovieri, F., Pirrone, N., Landis, M.S., Stevens, R.K. Atmospheric mercury behavior at different altitudes at Ny-Ålesund during Spring 2003. *Atmospheric Environ.* **2005b**, 39, 7646–7656. https://doi.org/10.1016/j.atmosenv.2005.08.001

(45) Sommar, J., Wängberg, I., Berg, T., Gårdfeldt, K., Munthe, J., Richter, A., Urba, A., Wittrock, F., Schroeder, W. H. Circumpolar transport and air-surface exchange of atmospheric mercury at Ny-Ålesund (79° N), Svalbard, spring 2002. *Atmos. Chem. Phys.* **2007**, 7, 151–166, doi:10.5194/acp-7-151-2007

(46) Ferrari, C.P., Padova, C., Faïn, X., Gauchard, P.-A., Dommergue, A., Aspmo, K., Berg, T., Cairns, W., Barbante, C., Cescon, P., Kaleschke, L., Richter, A., Wittrock, F., Boutron, C. Atmospheric mercury depletion event study in Ny-Alesund (Svalbard) in spring 2005. Deposition and transformation of Hg in surface snow during springtime. *Sci. Total Environ.* **2008**, 397, 167–177. https://doi.org/10.1016/j.scitotenv.2008.01.064

(47) Steen, A.O., Berg, T., Dastoor, A.P., Durnford, D.A., Engelsen, O., Hole, L.R., Pfaffhuber, K.A. Natural and anthropogenic atmospheric mercury in the European Arctic: a fractionation study. *Atmos. Chem. Phys.* **2011**, 11, 6273–6284. https://doi.org/10.5194/acp-11-6273-2011

(48) Angot, H., Dastoor, A., De Simone, F., Gårdfeldt, K., Gencarelli, C.N., Hedgecock, I.M., Langer, S., Magand, O., Mastromonaco, M.N., Nordstrøm, C., Pfaffhuber, K.A., Pirrone, N., Ryjkov, A., Selin, N.E., Skov, H., Song, S., Sprovieri, F., Steffen, A., Toyota, K., Travnikov, O., Yang, X., Dommergue, A. Chemical cycling and deposition of atmospheric mercury in polar regions: review of recent measurements and comparison with models. *Atmos. Chem. Phys.* **2016**, 16, 10735–10763. https://doi.org/10.5194/acp-16-10735-2016

(49) Landis, M.S., Stevens, R.K., Schaedlich, F., Prestbo, E.M. Development and Characterization of an Annular Denuder Methodology for the Measurement of Divalent Inorganic Reactive Gaseous Mercury in Ambient Air. *Environ. Sci. Technol.* **2002**, 36, 3000–3009. https://doi.org/10.1021/es015887t

(50) Steffen, A., Scherz, T., Olson, M., Gay, D., Blanchard, P. A comparison of data quality control protocols for atmospheric mercury speciation measurements. *J. Environ. Monit.* **2012**, 14, 752–765. https://doi.org/10.1039/C2EM10735J

(51) D'Amore, F., Bencardino, M., Cinnirella, S., Sprovieri, F., Pirrone, N. Data quality through a web-based QA/QC system: implementation for atmospheric mercury data from the global mercury observation system. *Environ. Sci.: Processes Impacts* **2015**, 17, 1482–1491. https://doi.org/10.1039/C5EM00205B

(52) Enrico, M., Le Roux, G., Marusczak, N., Heimburger, L.-E., Claustres, A., Fu, X., Sun, R., Sonke, J.E. Atmospheric mercury transfer to peat bogs dominated by gaseous elemental mercury dry deposition. *Environ. Sci. Technol.* **2016**, 50, 2405–2412. https://doi.org/10.1021/acs.est.5b06058

(53) Dunham-Cheatham, S.M., Lyman, S., Gustin, M.S. Evaluation of sorption surface materials for reactive mercury compounds. *Atmospheric Environ.* 2020, 242, 117836. https://doi.org/10.1016/j.atmosenv.2020.117836

(54) Miller, M.B., Dunham-Cheatham, S.M., Gustin, M.S., Edwards, G.C. Evaluation of cation exchange membrane performance under exposure to high Hg0 and HgBr2 concentrations. *Atmos. Meas. Tech.* **2019**, 12, 1207–1217. https://doi.org/10.5194/amt-12-1207-2019

(55) Biester, H. and Scholz, C. Determination of Mercury Binding Forms in Contaminated Soils: Mercury Pyrolysis versus Sequential Extractions. *Environ. Sci. Technol.* 1996, 31, 233-239. https://doi.org/10.1021/es960369h

(56) Stein, A.F., Draxler, R.R., Rolph, G.D., Stunder, B.J.B., Cohen, M.D., Ngan, F. NOAA's HYSPLIT

Atmospheric Transport and Dispersion Modeling System. *Bull. Ame. Meteorol. Soc.* **2015**, 96, 2059–2077. https://doi.org/10.1175/BAMS-D-14-00110.1

(57) Hersbach, H., Bell, B., Berrisford, P., Hirahara, S., Horányi, A., Muñoz-Sabater, J., Nicolas, J., Peubey, C., Radu, R., Schepers, D., Simmons, A., Soci, C., Abdalla, S., Abellan, X., Balsamo, G., Bechtold, P., Biavati, G., Bidlot, J., Bonavita, M., Chiara, G.D., Dahlgren, P., Dee, D., Diamantakis, M., Dragani, R., Flemming, J., Forbes, R., Fuentes, M., Geer, A., Haimberger, L., Healy, S., Hogan, R.J., Hólm, E., Janisková, M., Keeley, S., Laloyaux, P., Lopez, P., Lupu, C., Radnoti, G., Rosnay, P. de, Rozum, I., Vamborg, F., Villaume, S., Thépaut, J.-N. The ERA5 global reanalysis. *Q. J. R. Meteorol. Soc.* **2020**, 146, 1999–2049. https://doi.org/10.1002/qj.3803

(58) Boike, J., Juszak, I., Lange, S., Chadburn, S., Burke, E.J., Overduin, P.P., Roth, K., Ippisch, O., Bornemann, N., Stern, L., Gouttevin, I., Hauber, E., Westermann, S. Measurements in soil and air at Bayelva Station. Supplement to: Boike, J et al. (2018): A 20-year record (1998-2017) of permafrost, active layer and meteorological conditions at a high Arctic permafrost research site (Bayelva, Spitsbergen). *Earth Syst. Sci. Data*, **2017**, 10, 355-390, https://doi.org/10.5194/essd-10-355-2018.

(59) EMEP. Manual for sampling and chemical analysis, Norwegian Institute for Air Research, Kjeller, EMEP Report 1/95 (Last rev. 2001), https://projects.nilu.no/ccc/manual/index.html (last access: 12. April 2021)

(60) Hirdman, D., Aspmo, K., Burkhart, J.F., Eckhardt, S., Sodemann, H., Stohl, A. Transport of mercury in the Arctic atmosphere: Evidence for a spring-time net sink and summer-time source. *Geophys. Res. Lett.* **2009**, 36. https://doi.org/10.1029/2009GL038345

(61) Fisher, J.A., Jacob, D.J., Soerensen, A.L., Amos, H.M., Steffen, A., Sunderland, E.M. Riverine source of Arctic Ocean mercury inferred from atmospheric observations. *Nat. Geosci.* **2012**, 5, 499–504. https://doi.org/10.1038/ngeo1478

(62) Sonke, J.E., Teisserenc, R., Heimbürger-Boavida, L.-E., Petrova, M.V., Marusczak, N., Dantec, T.L., Chupakov, A.V., Li, C., Thackray, C.P., Sunderland, E.M., Tananaev, N., Pokrovsky, O.S. Eurasian river spring flood observations support net Arctic Ocean mercury export to the atmosphere and Atlantic Ocean. *PNAS* **2018**, 115, E11586–E11594. https://doi.org/10.1073/pnas.1811957115

(63) Gustin, M.S., Dunham-Cheatham, S.M., Huang, J., Lindberg, S., Lyman, S.N. Development of an Understanding of Reactive Mercury in Ambient Air: A Review. *Atmosphere* **2021b**, 12, 73. https://doi.org/10.3390/atmos12010073

(64) Horowitz, H.M., Jacob, D.J., Zhang, Y., Dibble, T.S., Slemr, F., Amos, H.M., Schmidt, J.A., Corbitt, E.S., Marais, E.A., Sunderland, E.M. A new mechanism for atmospheric mercury redox chemistry: implications for the global mercury budget. *Atmos. Chem. Phys.* **2017**, 17, 6353–6371. https://doi.org/10.5194/acp-17-6353-2017

(65) Peleg, M., Tas, E., Obrist, D., Matveev, V., Moore, C., Gabay, M., Luria, M. Observational Evidence for Involvement of Nitrate Radicals in Nighttime Oxidation of Mercury. *Environ. Sci. Technol.* **2015**, 49, 14008–14018. https://doi.org/10.1021/acs.est.5b03894

(66) Jiao, Y. and Dibble, T.S. First kinetic study of the atmospherically important reactions $BrHg^{\cdot}$ + NO2

and BrHg˙ + HOO. *Phys. Chem. Chem. Phys.* **2017**, 19, 1826–1838. https://doi.org/10.1039/C6CP06276H

(67) Lam, K.T., Wilhelmsen, C.J., Schwid, A.C., Jiao, Y., Dibble, T.S. Computational Study on the Photolysis of BrHgONO and the Reactions of BrHgO• with CH4, C2H6, NO, and NO2: Implications for Formation of Hg(II) Compounds in the Atmosphere. *J. Phys. Chem. A.* **2019**, 123, 1637–1647. https://doi.org/10.1021/acs.jpca.8b11216

(68) Dibble, T.S., Zelie, M.J., Mao, H. Thermodynamics of reactions of ClHg and BrHg radicals with atmospherically abundant free radicals. *Atmos. Chem. Phys.* **2012**, 12, 10271–10279. https://doi.org/10.5194/acp-12-10271-2012

(69) Toyota, K., McConnell, J.C., Lupu, A., Neary, L., McLinden, C.A., Richter, A., Kwok, R., Semeniuk, K., Kaminski, J.W., Gong, S.-L., Jarosz, J., Chipperfield, M.P., Sioris, C.E., 2011. Analysis of reactive bromine production and ozone depletion in the Arctic boundary layer using 3-D simulations with GEM-AQ: inference from synoptic-scale patterns. Atmospheric Chemistry and Physics 11, 3949–3979. https://doi.org/10.5194/acp-11-3949-2011

(70) Yang, X., Pyle, J.A., Cox, R.A., 2008. Sea salt aerosol production and bromine release: Role of snow on sea ice. Geophysical Research Letters 35. https://doi.org/10.1029/2008GL034536

(71) Huang, J., Jaeglé, L., Chen, Q., Alexander, B., Sherwen, T., Evans, M. J., Theys, N., and Choi, S., 2020. Evaluating the impact of blowing snow sea salt aerosol on springtime BrO and O3 in the Arctic, Atmos. Chem. Phys., 20, 7335–7358,https://doi.org/10.5194/acp-20-7335-2020.

(72) Simpson, W.R., Brown, S.S., Saiz-Lopez, A., Thornton, J.A., von Glasow, R. Tropospheric Halogen Chemistry: Sources, Cycling, and Impacts. *Chem. Rev.* **2015**, 115, 4035–4062. https://doi.org/10.1021/cr5006638

(73) Simpson, W.R., Glasow, R. von, Riedel, K., Anderson, P., Ariya, P., Bottenheim, J., Burrows, J., Carpenter, L.J., Friess, U., Goodsite, M.E., Heard, D., Hutterli, M., Jacobi, H.W., Kaleschke, L., Neff, B., Plane, J., Platt, U., Richter, A., Roscoe, H., Sander, R., Shepson, P., Sodeau, J., Steffen, A., Wagner, T., Wolff, E. Halogens and their role in polar boundary-layer ozone depletion. *Atmos. Chem. Phys.* **2007**, 7, 4375–4418. https://doi.org/10.5194/acp-7-4375-2007

(74) Abbatt, J.P.D., Thomas, J.L., Abrahamsson, K., Boxe, C., Granfors, A., Jones, A.E., King, M.D., Saiz-Lopez, A., Shepson, P.B., Sodeau, J., Toohey, D.W., Toubin, C., von Glasow, R., Wren, S.N., Yang, X. Halogen activation via interactions with environmental ice and snow in the polar lower troposphere and other regions. *Atmos. Chem. Phys.* **2012**, 12, 6237–6271. https://doi.org/10.5194/acp-12-6237-2012

(75) Foster, K.L., Plastridge, R.A., Bottenheim, J.W., Shepson, P.B., Finlayson-Pitts, B.J., Spicer, C.W. The Role of Br2 and BrCl in Surface Ozone Destruction at Polar Sunrise. *Science* **2001**, 291, 471–474. https://doi.org/10.1126/science.291.5503.471

(76) Liao, J., Huey, L.G., Liu, Z., Tanner, D.J., Cantrell, C.A., Orlando, J.J., Flocke, F.M., Shepson, P.B., Weinheimer, A.J., Hall, S.R., Ullmann, K., Beine, H.J., Wang, Y., Ingall, E.D., Stephens, C.R., Hornbrook, R.S., Apel, E.C., Riemer, D., Fried, A., Mauldin, R.L., Smith, J.N., Staebler, R.M.,

Neuman, J.A., Nowak, J.B. High levels of molecular chlorine in the Arctic atmosphere. *Nat. Geosci.* **2014**, 7, 91–94. https://doi.org/10.1038/ngeo2046

(77) Zhang, L. and Jaffe, D.A. Trends and sources of ozone and sub-micron aerosols at the Mt. Bachelor Observatory (MBO) during 2004-2015. *Atmospheric Environ.* **2017**, 165, 143–154. https://doi.org/10.1016/j.atmosenv.2017.06.042

(78) Pal, B. and Ariya, P.A. Studies of ozone initiated reactions of gaseous mercury: kinetics, product studies, and atmospheric implications. *Phys. Chem. Chem. Phys.* 2004, 6, 572–579. https://doi.org/10.1039/B311150D

(79) Lyman, S. N., Gustin, M. S., Prestbo, E. M. A passive sampler for ambient gaseous oxidized mercury concentrations. *Atmospheric Environ.* **2010**, 44, 246–252. https://doi.org/10.1016/j.atmosenv.2009.10.008

(80) Huang, J., Lyman, S.N., Hartman, J.S., Gustin, M.S. A review of passive sampling systems for ambient air mercury measurements. *Environ. Sci. Process Impacts* **2014**, 16, 374–392. https://doi.org/10.1039/c3em00501a

(81) Huang, J. and Gustin, M.S. Uncertainties of Gaseous Oxidized Mercury Measurements Using KCl-Coated Denuders, Cation-Exchange Membranes, and Nylon Membranes: Humidity Influences. *Environ. Sci. Technol.* **2015**, 49, 6102–6108. https://doi.org/10.1021/acs.est.5b00098

(82) Sprovieri, F., Pirrone, N., Bencardino, M., D'Amore, F., Angot, H., Barbante, C., Brunke, E.-G., Arcega-Cabrera, F., Cairns, W., Comero, S., Diéguez, M.D.C., Dommergue, A., Ebinghaus, R., Feng, X.B., Fu, X., Garcia, P.E., Gawlik, B.M., Hageström, U., Hansson, K., Horvat, M., Kotnik, J., Labuschagne, C., Magand, O., Martin, L., Mashyanov, N., Mkololo, T., Munthe, J., Obolkin, V., Ramirez Islas, M., Sena, F., Somerset, V., Spandow, P., Vardè, M., Walters, C., Wängberg, I., Weigelt, A., Yang, X., Zhang, H. Five-year records of mercury wet deposition flux at GMOS sites in the Northern and Southern hemispheres. *Atmos. Chem. Phys.* **2017**, 17, 2689–2708. https://doi.org/10.5194/acp-17-2689-2017

766

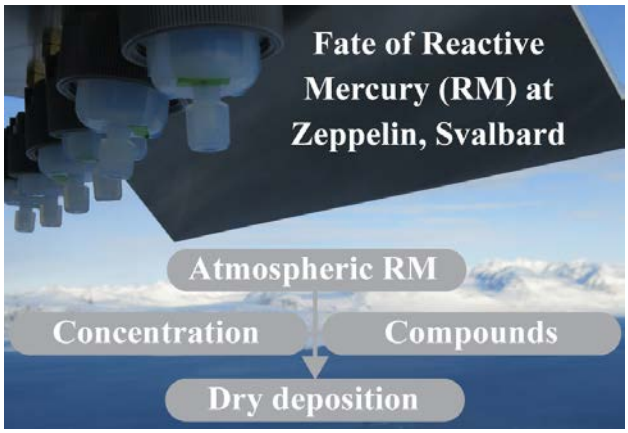
Fate of Reactive Mercury (RM) at Zeppelin, Svalbard
Atmospheric RM
Concentration
Compounds
Dry deposition

TOC

767